Department of Physics and Astronomy
University of Heidelberg

Bachelor Thesis in Physics
submitted by

Jan Felix Mücke

born in Friedberg (Germany)

2012

Triggering on light nuclei
with the
ALICE Transition Radiation Detector

This Bachelor Thesis has been carried out by Jan Felix Mücke at the
Physikalisches Institut of the University of Heidelberg
under the supervision of
Dr. Kai Schweda

iii

Abstract

In A Large Ion Collider Experiment (ALICE) at the Large Hadron Collider (LHC) protons are collided at a center-of-mass energy of currently 8 TeV. Collisions in which light (anti-)nuclei, such as the ^{3}He or ^{4}He (anti-)nucleus, are produced are extremely rare. The expected production yield in p-p collisions is in the order of 1 particle per 10^6 events. In order to study the production of light (anti-)nuclei a trigger - a mechanism to improve the signal to background ratio at aquisition time - is required. The specific energy loss of a charged particle passing through matter is proportional to the squared charge of the particle. This can be exploited as a trigger signature for particles with $z \geq 2$, recording only events that contain at least one track with a deposited energy higher than a treshold. In this thesis the feasibility of such a trigger for p-p collisions at level-1 (~ 8 μs after the collision) with the Transition Radiation Detector in ALICE was investigated. After promising results based on simulated data, a rejection and a trigger efficiency for $^3\overline{\text{He}}$ were extracted from real data.

Assuming a level-1 rate of 100 Hz and a level-0 rate of 20 kHz, which corresponds to a certain cut on the deposited charge, 10^6 seconds (~ 1 month) of data taking are expected to result in roughly 7000 $^3\overline{\text{He}}$ tracks in the recorded sample.

Kurzfassung

In A Large Ion Collider Experiment (ALICE) am Large Hadron Collider(LHC) werden Protonen mit einer Schwerpunktsenergie von 8 TeV zur Kollision gebracht. Die Produktion von leichten (Anti-)Kernen, d.h. von z.B. ^{3}He- oder ^{4}He-Kernen, in solchen Kollisionen ist extrem selten. Die erwartete Produktionsrate liegt in der Größenordnung von 1 Kern pro 10^6 Kollisionen, von denen nur ein Bruchteil aufgezeichnet werden kann. Um die Produktion dieser Kerne zu studieren wird also ein so genannter Trigger benötigt, ein System um online schnell zu entscheiden, welche Kollisionen aufgezeichnet werden. Der spezifische Energieverlust eines geladenen Teilchens in Materie ist proportional zum Quadrat seiner Ladung. Dies kann ausgenutzt werden, indem nur Kollisionen aufgezeichnet werden, welche mindestens eine Teilchenspur enthalten, deren deponierte Energie eine bestimmte Schwelle überschreitet. In dieser Arbeit wurde die Realisierbarkeit eines level-1 Triggers für Proton-Proton Kollisionen im Transition Radiation Detector in

ALICE untersucht, wobei level-1 bedeutet, dass die Entscheidung ca. 8 μs nach der Interaktion erfolgt. Nach viel versprechenden Simulationen wurde die Unterdrückung von Spuren, welche nicht von leichten Kernen verursacht worden sind, und die Trigger Effizienz basierend auf echten Daten berechnet. Nimmt man eine level-1 Rate von 100 Hz und eine level-0 Rate von 20kHz an, was einem bestimmten Schwellenwert bzgl. der deponierten Ladung entspricht, ergibt sich ein Erwartungswert von ca 7000 $^3\overline{\text{He}}$ Spuren in 10^6 Sekunden Datennahme (~ 1 Monat).

Contents

1. Introduction

With increasing beam energies and luminosities in particle and heavy ion physics experiments the possibility to study very rare physical processes arises. The Large Hadron Collider at the European Organization for Nuclear Research (CERN) has again pushed the boundaries of such studies to a new level. One of the physics processes which is not yet understood is the production of light nuclei in high energy collisions, especially in proton-proton collisions (p-p). In this thesis the term light nuclei refers to (anti-)nuclei with a baryon number of ±3 to ±4 and a charge of ±2e, e.g. the ^{3}He-nucleus. One model that makes predictions about the production yields of light nuclei is the Statistical Thermal Model [1]. A deconfined phase of matter is assumed at very high energies and densities, where quarks and gluons are not bound into hadronic states and can move freely. The so-called quark-gluon plasma is believed to have existed in the first microseconds of the Universe. At LHC energies this state lasts only for about 10^{-22} seconds. During the chemical freeze-out the free quarks and gluons hadronize and form the baryons and mesons which can then be detected in the experiment. The Statistical Thermal Model predicts that nuclei and anti-nuclei will be produced with equal abundancies during the hadronization phase at LHC energies [2]. Furthermore, it predicts that the production rate decreases by roughly a factor of 1000 for each additional (anti-)nucleon that is added to the (anti-)nucleus. This is supported by the $^4\overline{\text{He}}/^3\overline{\text{He}}$ ratio which was extracted via the measurement of 18 $^4\overline{\text{He}}$-nuclei in 10^9 Au+Au Collisions at $\sqrt{s_{NN}}$ = 200 GeV by the STAR collaboration [3].

   The expected deuteron yield for p-p collisions can be approximated based on a preliminary analysis of the deuteron production within the ALICE experiment as $2.4 \cdot 10^{-4}$ deuterons per unit of rapidity [4, 5]. With a predicted $^3\overline{\text{He}}/\text{d}$ ratio of about $7 \cdot 10^{-3}$ [6] at LHC energies, we roughly expect only about $1.7 \cdot 10^{-6}$ $^3\overline{\text{He}}$-nuclei per collision. In addition, just a fraction of the observed interactions can eventually be processed and recorded. To gather significant statistics it is therefore necessary to identify events containing light (anti-)nuclei during data taking. The goal of this thesis was to investigate the feasibility of such a filter mechanism (trigger) for light (anti-)nuclei in p-p collisions using the Transition Radiation Detector in ALICE.

After a short introduction of the experiment and the theoretical background in section 1 and 2, a feasibility study based on simulated data is presented in section 3. The main part of this analysis is described in section 4, where a rejection and trigger efficiency are extracted on the basis of real data from 2011 and 2012.

1.1. ALICE at the LHC

The Large Hadron Collider (LHC) [7] is the highest-energy and highest-luminosity hadron collider in the world and is located near Geneva at the European Organization for Nuclear Research (CERN). The collider ring is 26,7 km in circumference

and designed for a maximum center-of-mass energy of $\sqrt{s_{NN}} = 14$ TeV and a peak luminosity of $L = 10^{34}$ cm^{-2}s^{-1} in p-p collisions. It is also designed for lead-lead (PbPb) collisions with the goal of $\sqrt{s_{NN}} = 5.5$ TeV and $L = 10^{27}$ cm^{-2}s^{-1}.
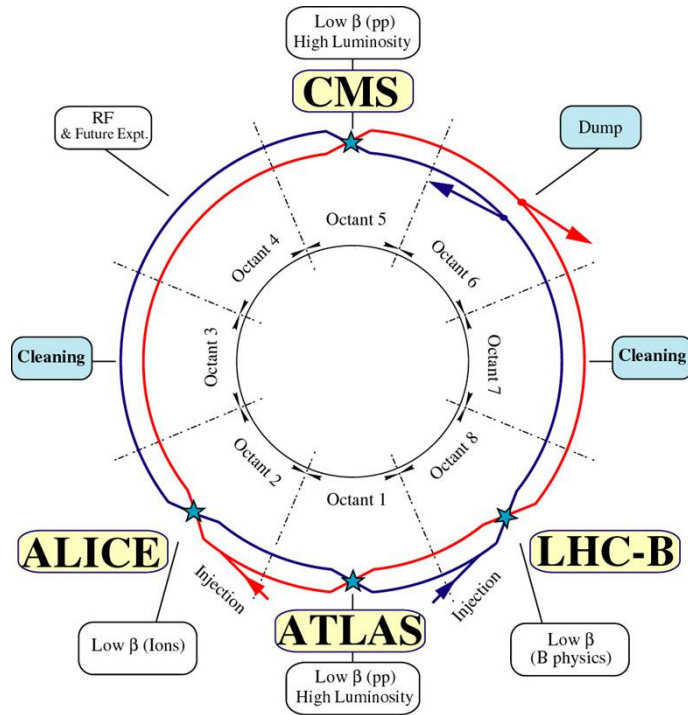

Figure 1: Schematic view of the Large Hadron Collider showing the position of the four main experiments. Figure taken from [7].

As illustrated in Fig. 1 there are four major experiments located along the beam pipe:

- **ATLAS** (A Toroidal LHC Apparatus):
  ATLAS [8] is a general purpose detector. Its main goal is the search for and the study of the Higgs Boson, also focusing on possible other massive vector bosons. CP violation, supersymmetry and additional dimensions are also topics in the program.

- **CMS** (Compact Muon Solenoid):
  CMS [9] has similar goals to the ATLAS experiment but uses different detector technologies.

- **LHCb** (LHC beauty):
  The LHCb experiment [10] is designed to investigate the CP violation in decay processes involving beauty quarks. One main goal is to investigate the matter-antimatter asymmetry which is still not understood within the standard model.

- **ALICE** (A Large Ion Collider Experiment):
  The ALICE experiment [11] is designed to handle the high multiplicities in lead-lead collisions. The main goal is to study and characterize the quark-gluon plasma, a deconfined phase of matter in which quarks and gluons are not bound in hadrons anymore.
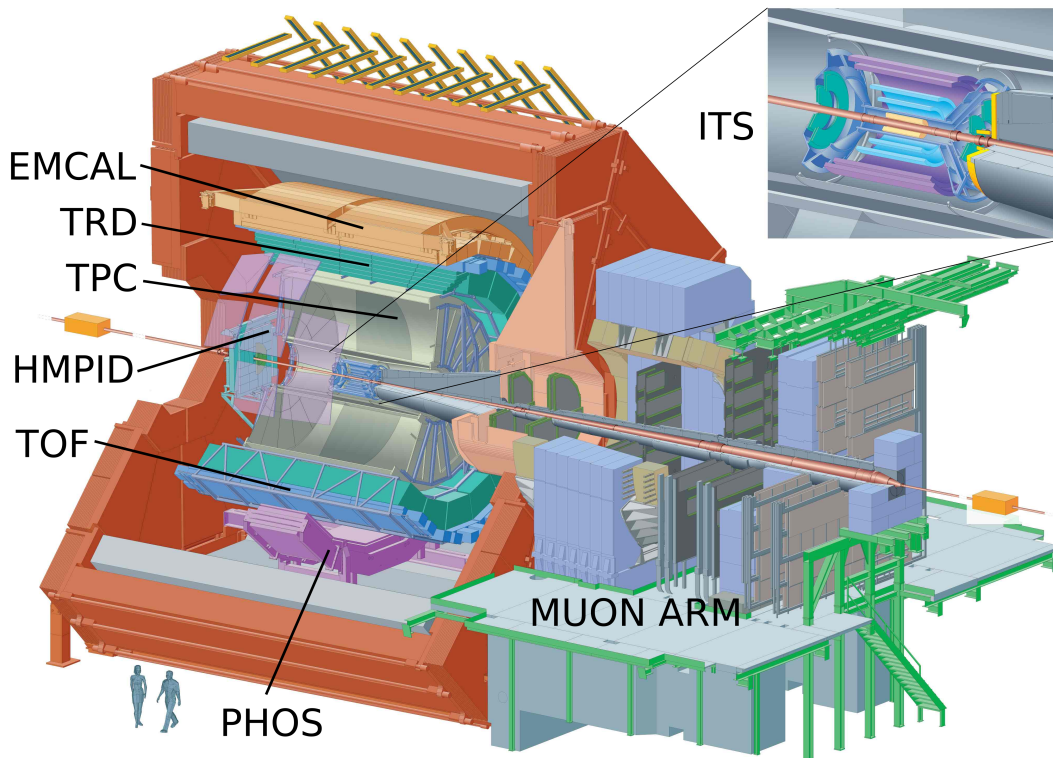

Figure 2: The ALICE Experiment. Figure taken from [12].

In Fig. 2 an overview of the ALICE experiment can be found. The detectors that are used in this analysis are described below:

- **ITS**
  The Inner Tracking System [11] consists of 6 silicon based detectors. With its high spatial resolution and small distance from the beam pipe it provides primary and secondary vertex information and allows the measurement of low transverse momenta.

- **TPC**
  The Time Projection Chamber [11] contributes most of the available tracking information in the ALICE central barrel. It allows the measurement of dE/dx with a resolution of about 5.2% in p-p and 6.5% in most central PbPb collisions [13].

- **TOF**
  The Time Of Flight detector [11] measures the arrival time of particles in the detector. In combination with the total momentum, the track length and the time of the primary interaction an estimation for the mass of a particle can be computed and used for particle identification.

- **TRD**
  The Transition Radiation Detector provides electron-pion separation and trigger contribution at level-1. Since the TRD plays a central role in this thesis it will be described in more detail in section 1.3.

1.2. Used variables and ALICE coordinate system

In Fig. 3 the ALICE coordinate system is defined. The z-axis points along the beam axis and away from the muon arm, the x-axis points towards the center of the collider ring. ϕ is the azimuthal angle relative to the x-axis, θ is the polar angle relative to the z-axis.
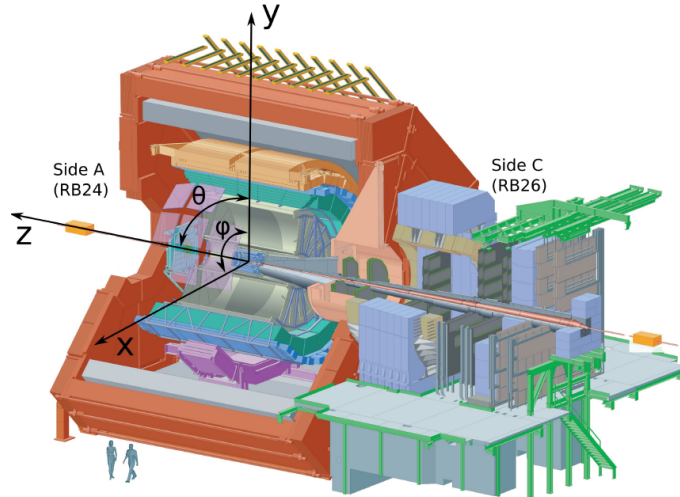

Figure 3: The ALICE coordinate system. Figure taken from [14].

Below two frequently used variables in collider physics are defined.

- p_T: The transverse momentum p_T is the projection of the total momentum of a particle on the x-y plane. Particle tracks are curved in the x-y plane due to the applied magnetic field in the central barrel. Through the measurement of the curvature, the transverse momentum can be reconstructed.

- y: The rapidity y is defined by: $y = \frac{1}{2}\ln\left(\frac{E+p_z c}{E-p_z c}\right)$, where E is the energy of a particle and p_z the component of its momentum along the beam axis. The difference of rapidities is independent of Lorentz boosts along the beam axis.

4

1.3. The Transition Radiation Detector

Two main design goals of the TRD are the separation of electrons and pions by transition radiation and to provide a trigger at level-1 [15]. If a highly relativistic particle ($\gamma \gtrsim 1000$) traverses the boundary between two media with different refractive indices, it can radiate a photon, preferably in the X-ray region (TR photon). Since the probability for the emission of such a photon is very small, many boundaries are needed. The radiator consists of a combination of polypropylene fibers and foam to fulfill these requirements.

In Fig. 4a a cross-section of a tracking chamber (x-z plane) is shown. A charged particle passing through the chamber deposits energy through ionization, resulting in clusters of electrons and ions. Due to an applied voltage the electrons drift towards the anode wires where the signal is amplified and the charge is induced to the read-out pads. The signal is proportional to the number of initially liberated electrons, i.e. the deposited charge. Deposited energy and deposited charge will be used synonymously in the following text. In case of the electron the effect of the previously described transition radiation photon is illustrated.
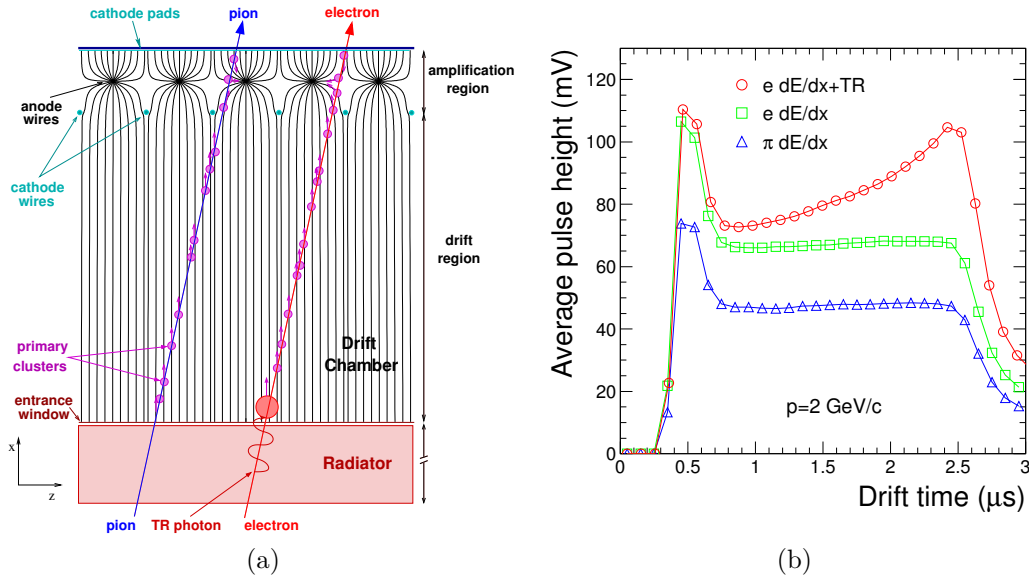
Figure 4: a)Schematic of a TRD tracking chamber. The radiator is facing the interaction point. Charged particles deposit charge through the ionization of the gas in the drift chamber. The charge then drifts to the read out electronics. Most electrons are highly relativistic and additionally emit a Transition Radiation photon which is absorbed at the entrance of the drift chamber. In b) the average pulseheight is plotted against the drift time. Transition Radiation leads to a characteristic peak at the end of the drift time (red curve). Figures taken from [16].

Due to the high photon absorption cross section of the gas in the drift chamber the TR photon deposits its energy close to the radiator in the drift region. The resulting pulseheight over time distribution, plotted in Fig. 4b, features a resulting characteristic peak at the end of the drift time for electrons which can be exploited

for particle identification. The peak at the beginning of the drift time is caused by the charge wich was deposited between the cathode pads and the anode wires.

The TRD is segmented in 18 supermodules, each consisting of 5 stacks of 6 tracking chambers. They are are arranged around the Time Projection Chamber (green in Fig. 2). [7]

1.3.1. Trigger system and online reconstruction

The interaction rate exceeds the feasible rate of data acquisition in ALICE (and in most of particle and heavy ion physics experiments). Thus, a mechanism is needed to identify "interesting" events (which can vary with the investigated physics question). This has to be done during data taking, before data is actually stored. A trigger in general is a system that performs such decisions. In ALICE three levels of hardware triggers are used.

After the data acquisition is started due to a signal at level-0 (L0) it can be aborted or continued based on contributions made at level-1 (L1) and level-2 (L2). Only fast detectors which are continuously sensitive to physics events contribute at level-0. In case of the TRD an additional pre-trigger system is installed inside the magnet responsible for the activation of the read-out electronics. This is necessary since the L0 signal arrives too late at the TRD after the interaction to wake up the electronics in time to record the full drift signal.
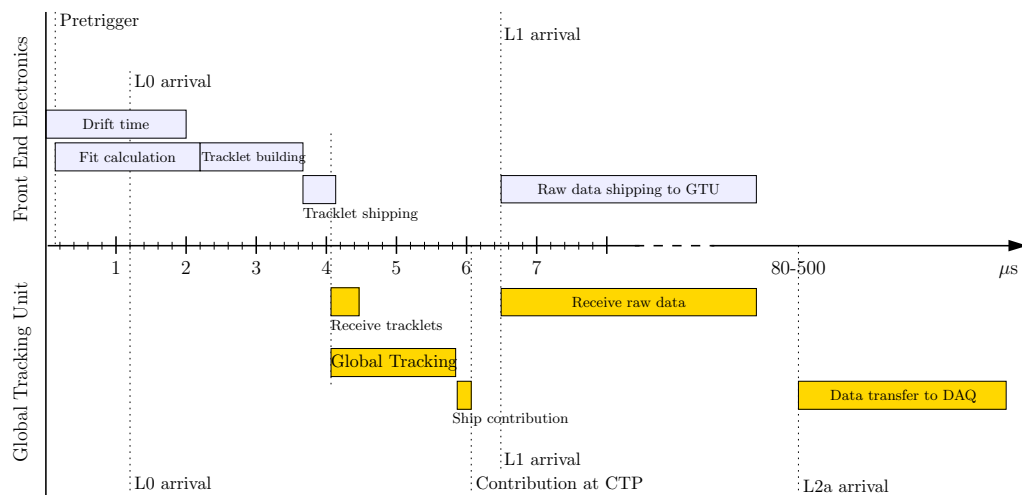

Figure 5: Overview of the trigger and reconstruction timing. Figure taken from [12].

After a L0 signal the detector is not sensitive to a new physics event until the processing of the current event is either completed or aborted. The L1 decision is issued only about 6.5 μs after L0 to keep the dead time low [17]. The L2 trigger contributes about 100 μs (drift time in the TPC) after the interaction and can provide more complex calculations based on data that was not yet sampled at L1. The last decision is made in the High Level Trigger (HLT), a high performance

PC cluster which is capable of advanced trigger algorithms and where the data is compressed. Accepted events are then saved to disk.

At the moment though every event that is accepted at L1 is also saved since L2 and the HLT currently accept every event.

The TRD contributes at level-1. A timing overview is given in Fig. 5. The first step is the chamber-wise tracking where tracklets are built out of the registered clusters in the tracking chambers. This process is already started during drift time. A straight line is fitted to each tracklet in the azimuthal plane and only tracklets whose angle relative to the radial axis does not exceed a defined value are then shipped to the Global Tracking Unit (GTU).
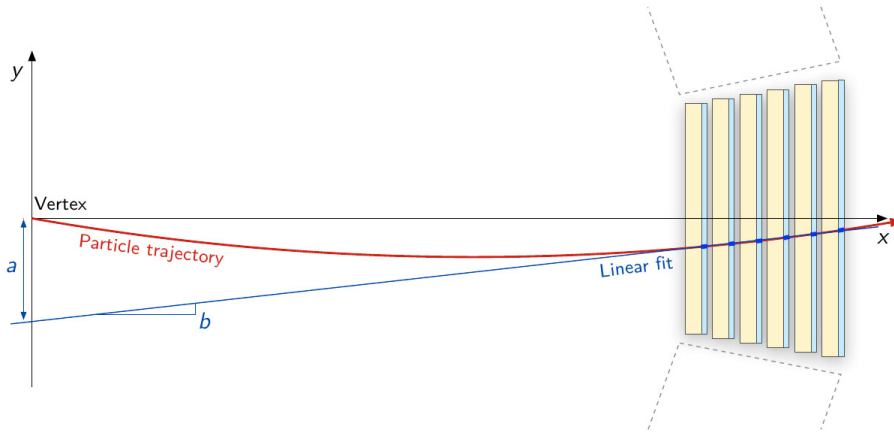

Figure 6: Schematic of the straight line fit which is performed to reconstruct the transverse momentum in the GTU. p_T is proportional to 1/a. Figure taken from [18].

Combinations of tracklets that are consistent with a track pointing to the primary vertex in the longitudinal direction are extended to a reference plane in the center of the associated stack. If the intersection points of at least 4 tracklets fall into a window of a given size, they form a track. Again a straight line fit is performed, this time to compute the transverse momentum as shown in Fig. 6. The mean of the deposited charge associated to the contributing tracklets is calculated and translated into the PID signal (Particle Identification). This is done using a nonlinear look-up table, where the characteristic charge deposition signatures produced by different particles are exploited to compute an electron likelihood. This will not be discussed any further since in this analysis a simpler approach is used as described later in section 2.3.

Tracks that are calculated in the GTU will be referred to as TRD tracks in the following text. Below the information which is contained in each TRD track at level-1 is listed.

7

- spatial position of the track

- transverse momentum

- PID signal (electron likelihood)

Table 1: Information contained in each TRD track at level-1.

2. Theoretical and technical background

2.1. Simulation with AliRoot

In this section the steps involved in a simulation with AliRoot [19] (the ROOT [20] based software framework used in ALICE) are described. The whole process from collision to the final output that can than be analysed is divided in 3 major parts. The first step is the physics simulation not involving any detector. The primary interaction vertex and the momenta of primary particles are calculated followed by the simulation of further decay processes. Several frameworks for this task (event generators) are available, differing in the implementation of the existing physical models that describe the underlying processes. PYTHIA 6 [21] is used for the simulation performed during this thesis.
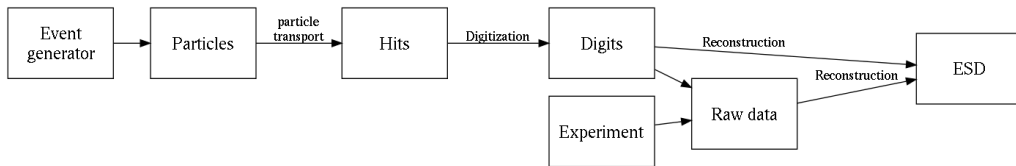

Figure 7: Simulation and reconstruction in AliRoot. Figure taken from [12].

In addition to the use of models that describe the collision based on propabilities one can place particles with fixed properties like the momentum and/or the direction in the event. One application is the simulation of particle cocktails, e.g. an underlying event enriched with high p_T tracks of α-particles. In the next step the particles are propagated through the detector which is done with GEANT 3 [22]. After the hits, i.e. the deposited energy in the detector, are calculated they are further processed to digitized values(digits) using the detector response. The result of the previous step contains all the data that is also included in raw data coming from real collisions. In case of simulated data additional Monte-Carlo information is also stored. During anlysis this allows to assign hits/digits and reconstructed tracks to the particle that produced them.

The last step, the reconstruction, is therefore identical for real and simulated data. Tracks are built out of digits and physics observables like the transverse momentum are calculated. The results are stored in the AliESD files (**E**vent **S**ummary **D**ata) and can then be analysed using the AliAnalysis framework [23].

2.2. Bethe formula

Let m_0 be the rest mass and p the momentum of a particle. The Bethe formula

$$-\left\langle \frac{dE}{dx} \right\rangle = Kz^2 \frac{Z}{A} \frac{1}{\beta^2} \left[\frac{1}{2} \ln\left(\frac{2m_e c^2 \beta^2 \gamma^2 T_{max}}{I^2} \right) - \beta^2 - \frac{\delta(\beta\gamma)}{2} \right] , \qquad (1)$$

9

with

$$\beta\gamma = \frac{p}{m_0} \qquad \beta = \frac{\beta\gamma}{\sqrt{1 + (\beta\gamma)^2}} \; , \tag{2}$$

describes the mean rate of energy loss of charged particles passing through matter. In the region of $0.1 \lesssim \beta\gamma \lesssim 1000$ it is accurate to a few percent [24].

T_{max} is the maximum kinetic energy which can be imparted to a free electron on a single collision. It is given by:

$$T_{max} = \frac{2m_e c^2 \beta^2 \gamma^2}{1 + 2\gamma m_e/M + (m_e/M)^2} \; . \tag{3}$$

A list of parameters is provided in table 2. In particle collision experiments the energy loss signatures described by the Bethe Formula are often used for particle identification. For this the knowledge of the absolute values of the mean rate of energy loss are not needed, but the differences between the various types of particles, i.e. the relative values.

Particles passing the detector essentially "see" the same materials, making material parameters uninteresting. Since the mass dependence of T_{max} is very weak it is a good approximation to treat it as proportional to $\beta^2\gamma^2$. The density effect correction $\delta(\beta\gamma)$ plays a minor role at the investigated velocity range ($\beta\gamma < 100$). This leaves the following dependencies:

$$-\left\langle \frac{dE}{dx} \right\rangle \approx az^2 \frac{1}{\beta^2} \left[\frac{1}{2} \ln\left(b\beta^4\gamma^4\right) - \beta^2 \right] \tag{4}$$
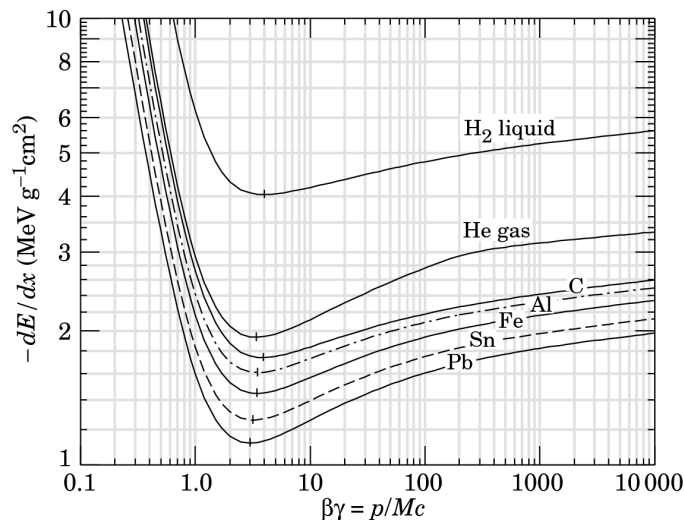
where a and b are constant.

Figure 8: Mean energy loss rate in different materials. Figure adapted from [24].

The Bethe formula does not differ for different kinds of particles if they move at the same $\beta\gamma$ through the detector (see Fig. 8). If one looks at the energy loss at a

given momentum, a clear separation, due to different rest masses and charge, can be observed and exploited for particle identification.

A result of such a measurement in the Time Projection Chamber of the ALICE experiment is presented in Fig. 9.
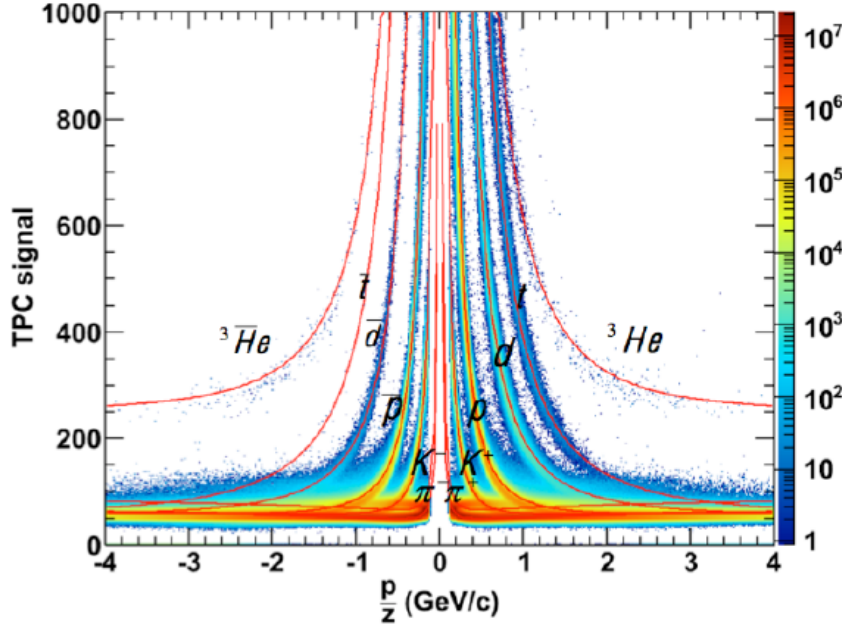

Figure 9: Measurement of dE/dx in the TPC, plotted over the rigidity which is defined by the ratio of total momentum and charge. Figure taken from [25].

Symbol	Definition	Units or Value
$m_e c^2$	electron mass $\times c^2$	0.510998918(44) MeV
N_A	Avogadro's number	$6.0221415(10) \times 10^{23}$ mol^{-1}
z	charge number of incident particle	
Z	atomic number of absorber	
A	atomic mass of absorber	gmol^{-1}
K	$4\pi N_A r_e^2 m_e c^2$	0.307075MeV cm^2 mol^{-1}
I	mean excitation energy	$\approx Z \cdot 10$eV
$\delta(\beta\gamma)$	density effect correction	

Table 2: Summary of variables used in this section. Table adapted from [24].

2.3. Charge deposition in the TRD

As described earlier, usually the deposited charge in each chamber gets translated into an electron likelihood (number between 0 and 255) using a nonlinear look-up table. Another possibility is to use a linear look-up table to scale the deposited

11

charge Q_0 to Q_s using a constant scaling factor c:

$$\text{PID signal} = \frac{Q_0}{c} = Q_s \; . \tag{5}$$

Q_s is assigned to each tracklet. Since tracks are built out of 4 to 6 tracklets, $\langle Q_s \rangle$ on track level is simply obtained by calculating the mean of Q_s measured in layer i:

$$\langle Q_s \rangle = \frac{1}{N} \sum_{i=0}^{N} Q_s^i \qquad \text{with } N = \text{number of contributing tracklets.} \tag{6}$$

The simulated data sample used for all further plots in this subsection is a cocktail of electrons, pions, protons, α-particles and their antiparticles with flat p_T distributions and identical abundances. A detailed description of the simulation can be found in section 3. If referred to a certain particle type later in this thesis, the corresponding antiparticle is also included unless specified otherwise.

In Fig. 10a the scaled charge distribution on tracklet level is plotted. The high peak at the right limit ($Q_s = 255$) is a result of the linear look-up table. If the deposited charge exceeds the highest entry, it still gets translated to 255. Therefore, the peak is the cumulated tail of the deposited charge distribution. In Fig. 10b one can see a similar plot, this time with separate curves for each simulated particle kind. The peaks are very broad on tracklet level, which explains that in Fig. 10a no structure, indicating a cocktail of different particle types, is visible. The dips in the curves are probably effects of the look-up table. Even though this is not fully understood yet, the impact on this analysis is negligible.
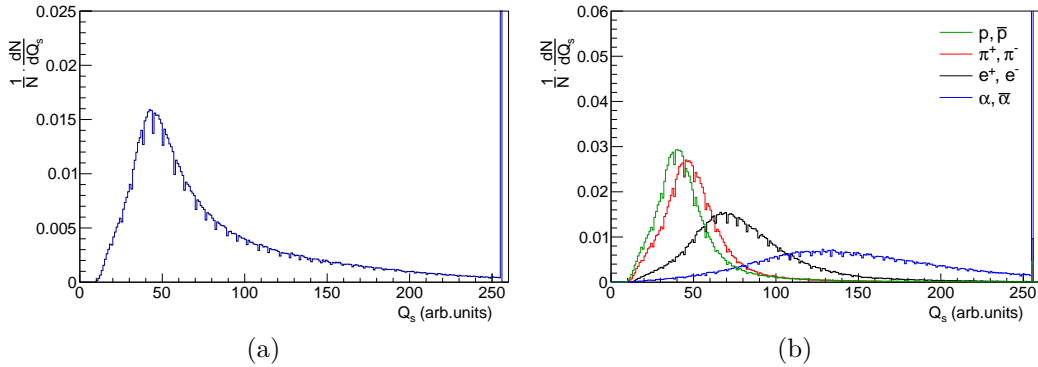

(a) (b)

Figure 10: Distribution of the scaled deposited charge Q_s on tracklet level for a) all tracklets, and b) for tracklets separated by particle kind. If the deposited charge of a tracklet exceeds the upper limit of the used linear look-up table, it is translated to $Q_s = 255$.

The same plots are extracted at the track level, after the mean calculation, and presented in Fig. 11a and 11b. One can clearly see that the transition from tracklet to track level improves the separation of the different curves. Again a peak a at $\langle Q_s \rangle = 255$ is present, produced by tracks where the maximum value of Q_s was assigned to all contributing tracklets.
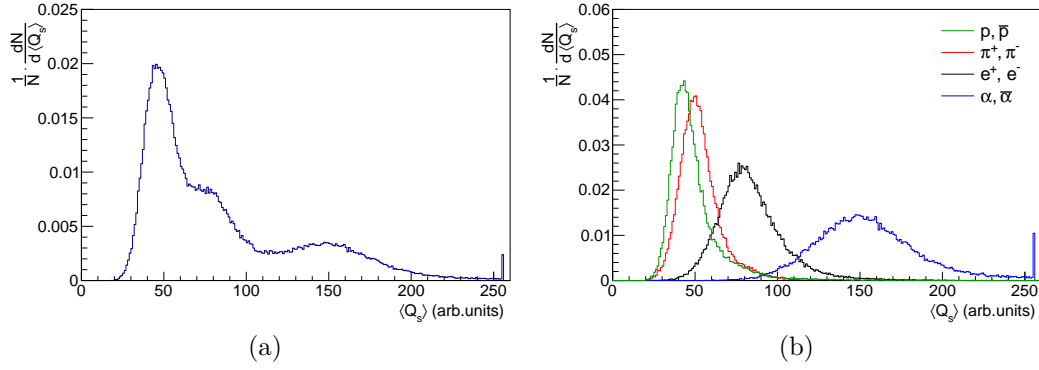
Figure 11: Distribution of the scaled deposited charge $\langle Q_s \rangle$ on track level for a) all tracks, and b) for tracks separated by particle kind.

2.4. Concept of this Trigger

In the previous section it was shown that there is a good separation between the $\langle Q_s \rangle$ peaks of α-particles and all other particles. This is expected since the Bethe formula is proportional to the squared charge of the particle passing the detector. The main idea of the light nuclei trigger is to set cuts on $\langle Q_s \rangle$ during data acquisition. This means to only process and store events that contain at least one TRD track with a $\langle Q_s \rangle$ higher than an earlier fixed threshold.
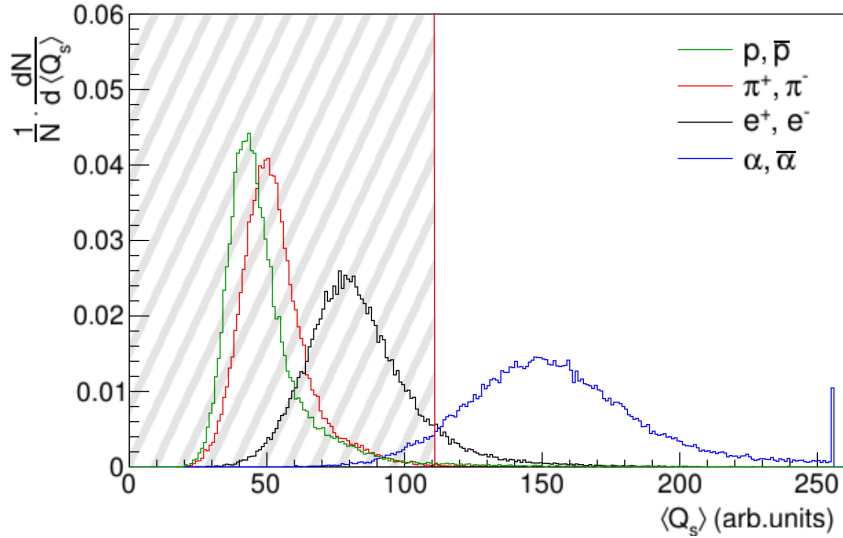
Figure 12: Main Idea: Only store events that contain at least one track with a higher $\langle Q_s \rangle$ than a fixed threshold. The red vertical line represents the cut on the deposited charge. The ruled area indicates suppressed tracks.

Based on Fig. 12 a cut on Q_s looks very promising for separation between α-particles

and others. To quantify the feasibility of a trigger one needs to compute an efficiency and a rejection which is done with simulated data in section 3 and again on real data in section 4.

3. Feasibility study based on simulations

In this section the proposed trigger concept is tested using simulated data which contains Monte-Carlo information. Even though the Monte-Carlo modeling is not perfect, this allows to trace back the source of an observed signal without any uncertainty.

3.1. Check of simulated energy deposition

The Bethe formula predicts that particles with $z = 2$ deposit 4 times more energy than particles with $z = 1$ if both are observed at the same $\beta\gamma$.

To check if this is modeled correctly and for later comparison with real data, a smaller sample was simulated where protons and α-particles were aimed at the TRD perpendicular to the beam axis with a fixed $\beta\gamma$ of 4.25. This translates to $p_T \approx 4$ GeV/c for protons and $p_T \approx 16$ GeV/c for α-particles. This value was chosen rather randomly, the only concern was to simulate in the maximum efficiency range of the TRD which starts above about 2.5 GeV/c. The resulting scaled charge distributions are plotted in Fig. 13.

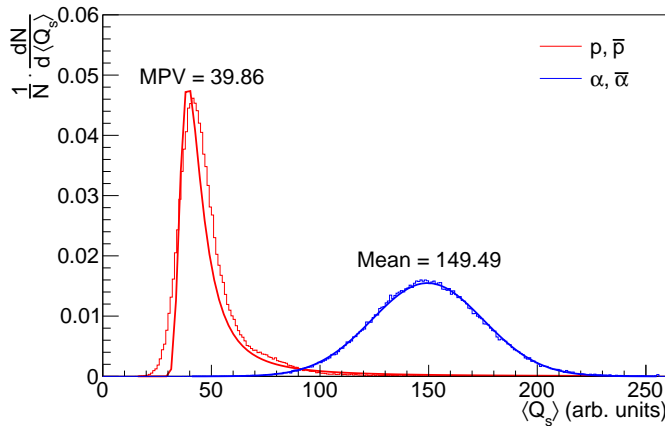Figure 13: Scaled charge distributions of protons and α-particles in the TRD, both simulated with $\beta\gamma = 4.25$. The ratio of the x-position of the maxima is 3.69, compared to a factor of 4 which is predicted by the Bethe formula. Statistical errors are smaller than 1 ‰.

The blue curve, produced by α-particles, can be well described by a normal distribution. A Landau distribution [24] was fitted to the red curve, which was produced by protons. The ratio of the x-positions of the two maxima is 3.69, statistical errors are smaller than 1 ‰.

3.2. Data sample

There was no simulated data including light nuclei and the simulation of trigger processing available. That means the available data did not contain TRD tracks

15

and tracklets. Since we want to apply cuts on the deposited charge in the TRD, a new simulation was necessary that includes the processes performed online during data taking in the TRD[1].

The resulting data sample is a cocktail of protons, electrons, α-particles and their antiparticles. Furthermore negative and positive pions are included.

The cocktail was simulated with a flat p_T-distripution which allows analysis with equally good statistics in the whole investigated p_T-range.

The measurement of p_T is done through the measurement of the bending of a track. The Lorentz force is proportional to the particle charge z. Therefore, lacking the knowledge of z during reconstruction, a real value p_T results in a measured value of p_T/z (rigidity). To achieve equal rigidity distributions for all particle types protons, electrons and pions were simulated with p_T ranging from 0 to 10 GeV/c and α-particles ranging from 0 to 20 GeV/c. In table 3 an overview of the sample is provided.

number of events	10000	
number of particles per event and type	10	
p_T-range (anti-)α-particles	0 - 20 GeV/c	flat
p_T-range others	0 - 10 GeV/c	flat

Table 3: Simulation summary

3.3. Rejection and Efficiency

Let N_t be the total number of global tracks of particle type t and $N_t(\langle Q_s \rangle > X)$ the number of TRD tracks that passed the cut on $\langle Q_s \rangle$ at X. The scaled deposited charge $\langle Q_s \rangle$ is only a feature of TRD tracks, since it is computed online in the GTU as described in section 1.3. Thus, a cut on $\langle Q_s \rangle$ affects only the set of TRD tracks which forms the base set for $N_t(\langle Q_s \rangle > X)$. N_t on the other hand is a subset of the so called ESD tracks which are computed during offline reconstruction. Data coming from multiple detectors is used to form a track during this process. It happens frequently that a particle is e.g. registered in the TPC/ITS (and therefore an ESD track can be formed) but not in the TRD, mainly due to two effects:

- **acceptance**: Currently only 13 of 18 supermodules are installed. In addition there are small gaps between the supermodules. In other words the TRD does not provide full azimuthal coverage. Tracks found in the TPC and ITS can be located outside the TRD acceptance.

- **tracking efficiency**: Also the TRD tracking efficiency is strongly dependent on the transverse momentum. The TRD can not detect particles with low

---

[1]The part where the cocktail is implemented in the *Config.C* can be found in appendix A

p_{T} since those particles never reach the detector due to their bending in the magnetic field. Therefore, the tracking efficiency starts to rise around 0.5 GeV/c and saturates at about 2.5 GeV/c.

To emphasize the different base sets of N_t and $N_t(\langle Q_s \rangle > X)$ those quantities will be referred to as N_t^{ESD} and $N_t^{TRD}(\langle Q_s \rangle > X)$ from now on.

As mentioned before the two quantities needed to discuss the feasibility of a trigger are the rejection and the efficiency. The rejection $r_t(\langle Q_s \rangle)$ describes how many unwanted tracks of particle type t pass the cut and therefore fire the trigger, compared to their total number and is given by:

$$r_t(\langle Q_s \rangle) = \frac{N_t^{TRD}(\langle Q_s \rangle > X)}{N_t^{ESD}} \ . \tag{7}$$

If the rejection is computed for the particle type that is supposed to be selected by the trigger, in this case that is $t = \alpha$, it becomes the efficency:

$$\epsilon_\alpha(\langle Q_s \rangle) = \frac{N_\alpha^{TRD}(\langle Q_s \rangle > X)}{N_\alpha^{ESD}} \ . \tag{8}$$

$\epsilon_\alpha(\langle Q_s \rangle)$ contains the tracking efficency but adds the effect of the applied cut on $\langle Q_s \rangle$.

In this section the rejection and the efficiency are obtained on track level. This means that single tracks are rejected or accepted and not whole events. Since it is extremely unlikely to find more than one $^{3/4}$He-track in one real event and other tracks in an event containing a $^{3/4}$He-track can also fire the trigger, the above defined efficiency on track level is a lower bound estimation for the real efficency on event level.

An exact modelling of the rejection on event level is not intended nor neccesary since the rejection can be easily extracted with high accuracy from real data. The computed rejection on track level shows if a separation of $^{3/4}$He-tracks and other tracks can be achieved with the discussed cuts on the scaled charge.

3.4. Results

In Fig. 14 the rejection for electrons and pions at different cuts on $\langle Q_s \rangle$ is plotted. Electrons are especially critical due to their high charge deposition and therefore high chance to falsely fire the trigger. Pions deposit far less energy but the majority of tracks in p-p collisions are pions. The global rejection, i.e. the rejection of all tracks that are not α-particles, lies between the electron and pion rejection.
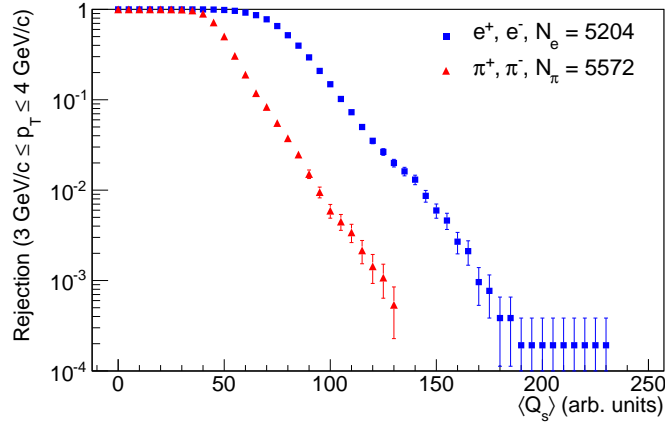
Figure 14: Rejection of pions and electrons plotted vs. different cuts on the scaled charge. Tracking efficiency and acceptance are not included.
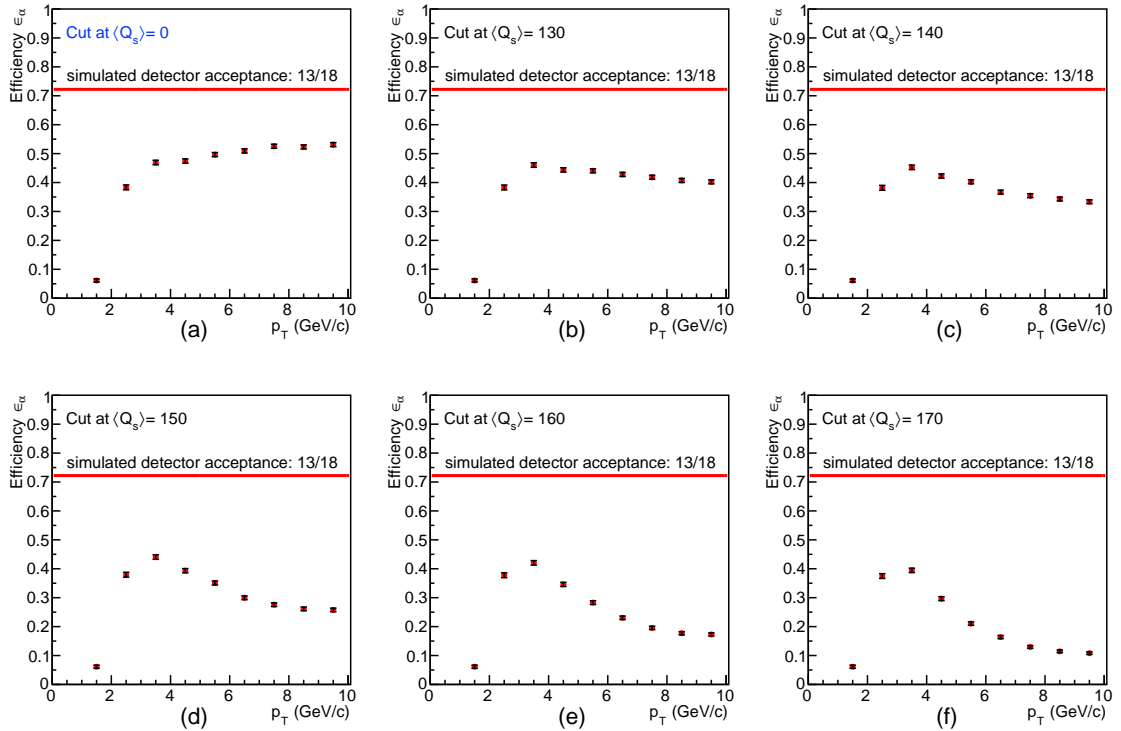

Figure 15: Efficiency ϵ_α plotted against the transverse momentum for different cuts. In (a) the combined tracking efficiency and acceptance of the TRD is shown since no cut on the scaled charge is applied. The red lines indicate the idealised acceptance since 13 of 18 supermodules are currently installed and were simulated. Further losses are mostly due to gaps between the supermodules and edge effects.

In Fig. 15 the efficiency for different $\langle Q_s \rangle$-cuts is plotted against the transverse momentum. Figure 15a shows the effect of the combined acceptance and tracking

efficency since no cut on $\langle Q_s \rangle$ was applied. Starting at Fig. 15b, with an applied cut at $\langle Q_s \rangle = 130$, the cuts grow in steps of ten, resulting in a maximum cut at $\langle Q_s \rangle = 170$ in Fig. 15f. Compared to lower cuts the curves drop only slightly in the p_T-region from 2 GeV/c to 4 GeV/c but much stronger in higher p_T-regions. The explanation for this behaviour is the p_T-dependence of the charge deposition of alphas plotted in Fig. 16. Due to their mass of 3.73 Gev/c^2 a momentum below 3.73 Gev/c translates to a $\beta\gamma$ below 1, where the Bethe curve is growing fast towards lower values of $\beta\gamma$. As a result almost all TRD tracks that are found in the p_T-region between 2 GeV/c and 4 GeV/c survive the cut on $\langle Q_s \rangle$ which leads to the nearly constant efficiency in this p_T-region. TRD tracks with higher momentum deposit less energy and therefore are affected stronger by the $\langle Q_s \rangle$-cuts.

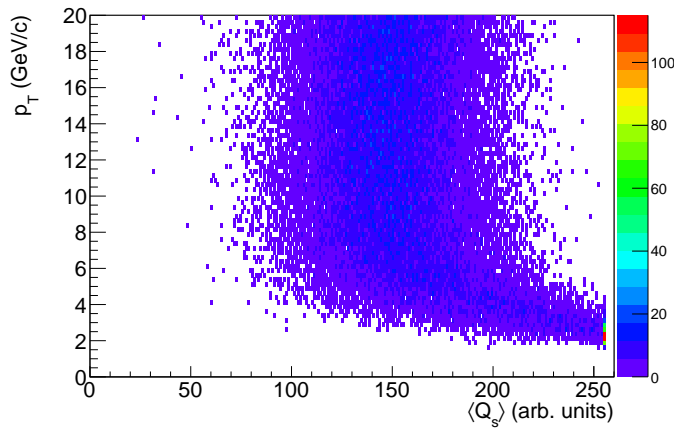

Figure 16: Transverse momentum versus deposited charge of α tracks.

3.5. Possible improvements of rejection

To improve the separation of the deposited charge curves shown in Fig. 12, and therefore the rejection of non-^{4}He tracks at constant efficency, two approaches were investigated.

3.5.1. p_T-Cuts

One idea was to only look at tracks above a certain transverse momentum. The motivation for this can be found in Fig. 9. In regions of low momenta the specific energy loss curves of different particles are less separated than in higher momentum regions. A cut on p_T is supposed to suppress exactly those less separated regions and therefore improve separation/rejection.
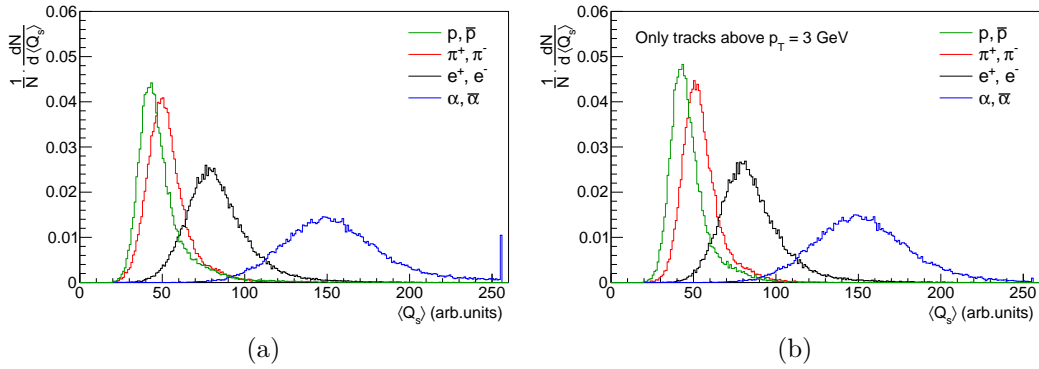
Figure 17: a) Distribution of the scaled charge for all tracks separated by particle kind. Identical to Fig. 11b, shown for comparison. b) As a) but only for tracks above $p_\mathrm{T} = 3$ GeV/c.

The resulting scaled charge distributions, after a p_T-cut at 3 GeV/c was applied, are plotted in Fig. 17b, next to the previously shown distribution without p_T-cut. The most obvious difference between the plots is the missing peak at $Q_s = 255$. As explained above α-particles with low momentum deposit the largest amounts of energy in the detector. Those tracks are suppressed by the p_T-cut. This is an undesired effect because a lot of tracks are lost that would correctly fire the trigger. In addition, the separation is not significantly improved. While Fig. 9 suggests a very big effect, one has to keep in mind that the online tracking in the TRD is inefficient for tracks with transverse momenta below 2 GeV/c. Therefore, just a small fraction of the theoretically suppressed tracks is detected in the TRD anyway.

3.5.2. Truncated mean

Usually the deposited charge associated with a TRD track is the mean of the deposited charge of the contributing tracklets as explained in section 2.3. A different approach is to use a truncated mean. In general this means to discard parts of a given sample at the low and/or high end in similar or different proportions. In this case the goal is to reduce the tail of the scaled charge distributions and improve separation. Therefore, at the transition from tracklet to track level, the tracklet with the highest $\langle Q_s \rangle$ is not taken into account during mean calculation. In Fig. 18b, next to the already introduced $\langle Q_s \rangle$-distribution (normal mean) for comparison, the result of this truncated mean calculation is plotted.
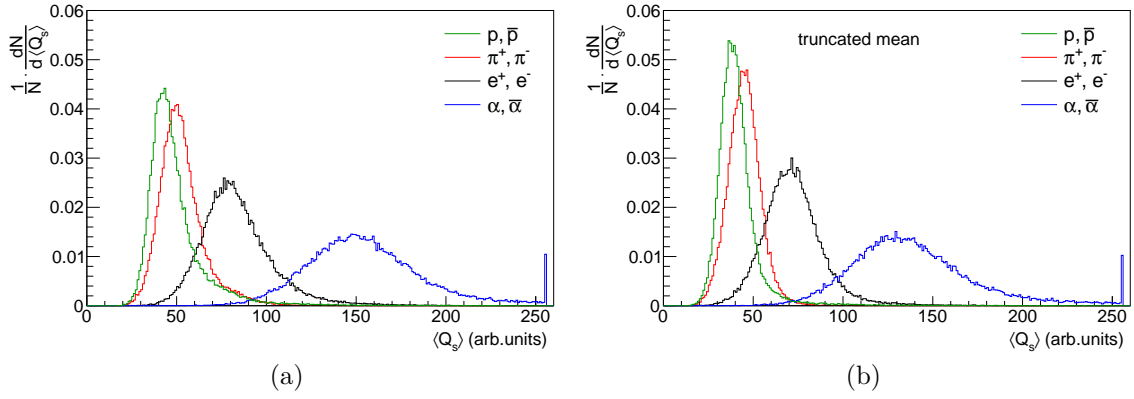
Figure 18: a) Distribution of $\langle Q_s \rangle$ for all tracks separated by particle kind. Identical to Fig. 11b, shown for comparison. b) As a) but the $\langle Q_s \rangle$ on track level was calculated using a truncated mean.

Two effects are visible. Especially the proton and pion peak are higher and narrower. Also all peaks are shifted to lower values of $\langle Q_s \rangle$. To quantifiy any possible improvement, pairs of rejection and trigger efficiency, obtained in the p_T-interval 3 GeV/c - 4 GeV/c for different $\langle Q_s \rangle$-cuts, were plotted in Fig. 19. The curves are very similar, no improvement of the rejection is observed in the interesting range between a cut on $\langle Q_s \rangle$ at 90 and 160.
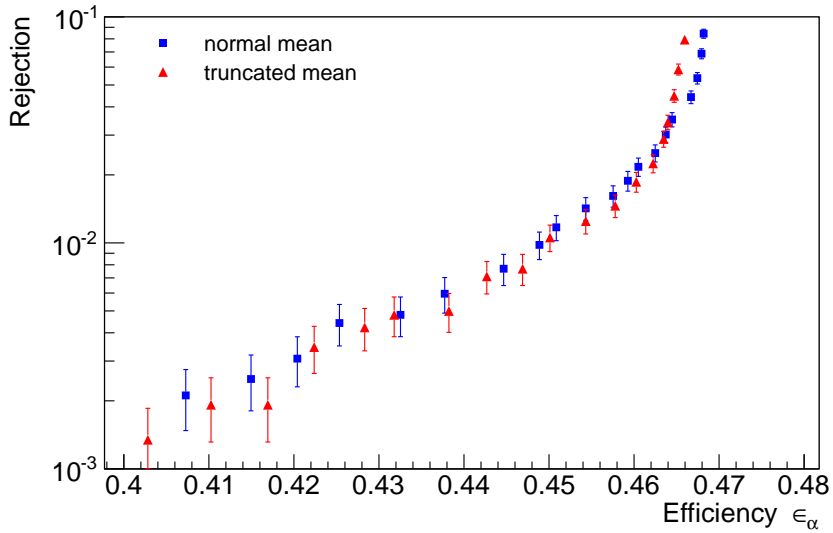

Figure 19: Plotted are pairs of electron rejection and α-efficiency in the p_T-range from 3 GeV/c to 4 GeV/c. Each pair belongs to a certain $\langle Q_s \rangle$-cut between 90 and 160. Relative x-errors lie between 1.7% and 1.9% and are not plotted.

21

4. Feasibility study on real data

Based on the results presented in the previous section the trigger looks promising. Nevertheless the simulation was just a first approximation of the real rejection and efficiency during data taking. Especially the global rejection on event level is expected to look different than the rejections on track level computed before.

In this section the efficiency and the rejection are extracted again, this time using real data and therefore lacking Monte-Carlo information. As mentioned before this trigger is supposed to be used during p-p collisions. Hence a p-p run is used to compute the rejection. For the efficiency the situation is more complicated. No p-p data sample was available with a sufficient number of $^{3/4}$He included to achieve significant statistics. Therefore, the PbPb data from 2011 was used to obtain the efficiency.

4.1. Rejection

As mentioned during the introduction usually the deposited charge of tracks in the TRD gets translated to an electron likelihood during data taking, using a non linear look-up table. This look-up table is not monotonous which prevents the reverse calculation. Therefore, run 176730 was used to extract the rejection since a linear look-up table was used in this run.

During data taking whole events are rejected or recorded, not single tracks. One track with a deposited charge above the choosen cut is sufficient to accept the event, independent of the particle kind. Let N_{event} be the number of all events with fired pre-trigger, i.e. TRD read-out, and $N_{event}(\langle Q_s \rangle > X)$ be the number of events additionally containing at least one track with $\langle Q_s \rangle$ higher than the chosen cut at X. Due to the very small ^{3}He-yield of approximately $1.7 \cdot 10^{-6}$ ^{3}He tracks per event in p-p, it is a good approximation to assume that no ^{3}He or ^{4}He track is included in the sample. The rejection r on event level is then determined by:

$$r = \frac{N_{event}(\langle Q_s \rangle > X)}{N_{event}} \ .$$

(9)

The results are plotted in Fig. 20. Even with no applied cuts on the deposited charge the rejection is never 1 (no event rejected) since only about 40% of events with fired pre-trigger, i.e. with TRD read-out, actually contained TRD tracks. This is expected due to the low multiplicities (in average 7 primary tracks per event) in p-p collisions and the steeply falling p_T-spectra and is not a malfunction of the TRD. If compared to the simulated distributions of $\langle Q_s \rangle$ presented in e.g. Fig. 12, the observed rejection at $\langle Q_s \rangle$-cuts above 200 is weaker (closer to 1) than expected. Many photons convert to electron positron pairs right before they enter the TRD. Since electrons(positrons) naturally deposit high amounts of energy and the majority of all electrons(positrons) registered in the TRD comes from photon conversions, they are expected to be the main source of background with high energy deposition that fires the trigger. Only photons coming from secondary interactions

were included in the simulated sample described in section 3.2, so essentially the described effect was not included in the simulation.
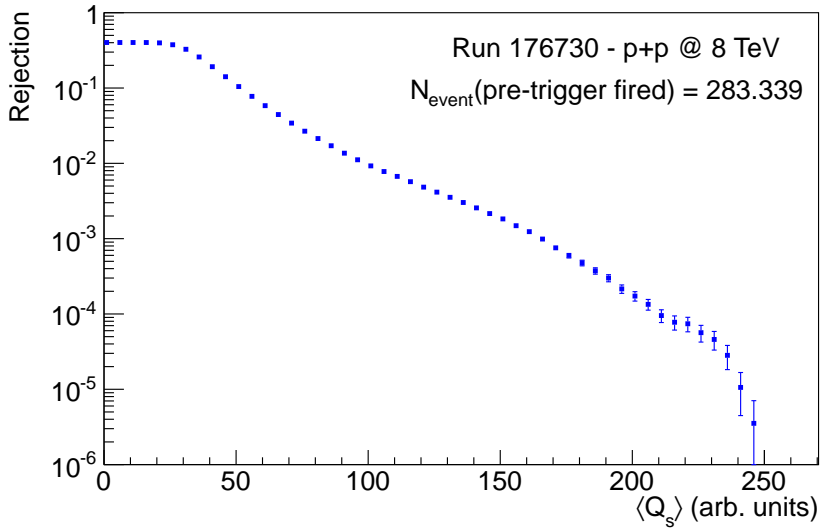

Figure 20: Rejection for different cuts on the deposited charge.

4.2. Efficiency

4.2.1. Data sample

For a particle with momentum p, rest mass m_0 and charge z the most probable energy loss in the TPC can be calculated using the ALEPH parametrization [26]:

$$f(\beta\gamma, z) = z^2 \frac{\lambda_1}{\beta^{\lambda_4}} \left[\lambda_2 - \beta^{\lambda_4} - \ln\left(\lambda_3 + \frac{1}{(\beta\gamma)^{\lambda_5}} \right) \right] . \tag{10}$$

The parameters λ_i depend on the calibration of the TPC and are experimentally determined. The paramaters [27] used for this analysis can be found in appendix C. Assuming different particle types, i.e. rest mass and charge, expected TPC signals can be calculated for each track with momentum p and utilized for particle identification. If the measured TPC signal of a track lies within a 20% range of an expected signal, the track is flagged as a candidate for the assumed particle type. A 20% range is about equivalent to a 3σ cut since the TPC signal can be described by a normal distribution for a fixed momentum and particle type [26].
Using a similar method the PbPb data from 2011 was searched for events containing a $^{3/4}\overline{\text{He}}$ candidate. For each track the expected TPC signal, assuming ^{3}He rest mass and charge, was calculated. Each event, containing at least one track with negative charge (indicated by the bending direction of the track) and with a measured TPC signal higher than 0.8 times the expected one, was flagged. All flagged events were merged and form the sample used in this analysis. Additionally the tracking

23

that is performed online in the GTU was redone offline since a major fraction of all tracks was lost due to time-outs during online tracking. This resimulation resulted in a set of TRD tracks roughly bigger by a factor of 4, compared to the number of TRD tracks which could be calculated online and was already included in the Event Summary Data.
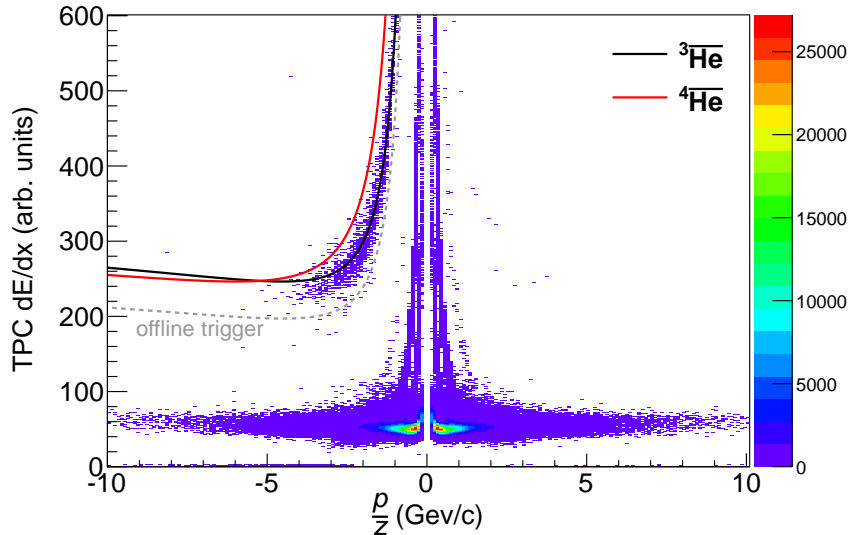

Figure 21: TPC dE/dx vs rigidity distribution for events (PbPb, 2011) passing the offline trigger selection of events with at least one $^{3/4}\overline{\text{He}}$ candidate. Additionally, further quality cuts were applied (see appendix B). The black and red curve represent the ALEPH parametrizations of the specific energy loss of $^3\overline{\text{He}}$ and $^4\overline{\text{He}}$ that were used for particle identification.

In Fig. 21 the TPC dE/dx vs rigidity distribution of all tracks that survived further quality cuts (see appendix B), which were applied to exclude unphysical tracks, is plotted. The gray dashed line indicates the applied offline cut during selection. The parametrizations of $^{3/4}\overline{\text{He}}$ are also plotted in Fig. 21 as the blue and red lines. It is clearly visible that they are very similar, $^3\overline{\text{He}}$ and $^4\overline{\text{He}}$ can not be separated with cuts on dE/dx alone. Nearly all of the light anti-nuclei in this sample are $^3\overline{\text{He}}$ tracks [4]. Therefore, the trigger efficiency will be extracted with $^3\overline{\text{He}}$ candidates. The weak separation between the energy loss signatures of $^3\overline{\text{He}}$ and $^4\overline{\text{He}}$ leads to two things. Firstly, the set of $^3\overline{\text{He}}$ candidates might very well contain some $^4\overline{\text{He}}$ tracks; secondly, this does not affect the resulting efficiency in any significant way.
In Fig. 21 also a few $^{3/4}$He candidates in the positive z area are visible. During analysis tracks with positive and negative charge were not discriminated. Therefore, a small fraction of the $^3\overline{\text{He}}$ candidates might actually be ^{3}He candidates. Since this has no significant impact on the results and the majority of tracks have negative charge, all candidates will be referred to as $^3\overline{\text{He}}$ candidates.

4.2.2. Matching of ESD and TRD tracks

Since the above explained particle identification uses the TPC signal, $^3\overline{\text{He}}$ candidates are ESD tracks. To assign a value of $\langle Q_s \rangle$ and then apply cuts, they have to be matched to a TRD track. The used matching algorithm was developed by Felix Rettig and slightly modified for integration in this analysis. The spatial distance and the difference in transverse momentum of ESD and TRD tracks form the criteria for a match rating between 0 (no match) and 1 (best match). The first step during analysis is to identify $^3\overline{\text{He}}$ candidates. If a $^3\overline{\text{He}}$ candidate is found, a match rating is computed for every TRD track contained in the corresponding event.
The match rating algorithm is divided in two functions:

- `EstimateTrackDistance(ESD track, TRD track)`: The spatial distances in y and z direction between the 4 to 6 tracklets that form the track and the ESD track are computed, using the anode plane in the layer where the respective tracklet is located as a reference plane. The spatial distances are then averaged over the contributing layers resulting in the spatial distance in y- and z-direction $|\triangle y|$ and $|\triangle z|$.

- `RateTrackMatch(`$|\triangle y|$`, `$|\triangle z|$`, `p_T^{ESD}`, `p_T^{TRD}`)`: Taking into account the difference in granularity in y- and z-direction rating factors for the spatial distances are computed as follows:

$$
f_z = \begin{cases} 0 & |\triangle z| > 20 \\ -0.025 \cdot |\triangle z| + 1 & |\triangle z| \leq 20 \end{cases}, \tag{11}
$$

$$
f_y = \begin{cases} 0 & |\triangle y| > 5 \\ -0.1 \cdot |\triangle y| + 1 & |\triangle y| \leq 5 \end{cases}. \tag{12}
$$

The rating factor for the transverse momenta is given by:

$$
f_{p_T} = 1 - \frac{|p_T^{ESD} - p_T^{TRD}|}{p_T^{ESD}} . \tag{13}
$$

If f_{p_T} is negative, 0.2 is assigned to exclude negative ratings. The final rating factor f_r is the product of all factors:

$$
f_r = f_z \cdot f_y \cdot f_{p_T} \tag{14}
$$

Pairs of ESD and TRD tracks with a match rating higher than 0.3 are considered as matched tracks. In case of more than one good match, the best matching pair is used in further analysis.

4.2.3. Results

Let $N_{3\overline{\text{He}}}^{ESD}$ be the number of all $^3\overline{\text{He}}$ candidates, and $N_{3\overline{\text{He}}}^{TRD}(\langle Q_s \rangle > X)$ the number of $^3\overline{\text{He}}$ candidates that could be matched to a TRD track with a $\langle Q_s \rangle$ bigger than the applied cut at X. In the p_{T}-range of p_{T}^{thr} to $p_{\text{T}}^{thr} + 1$ GeV/c the efficiency is given by:

$$\epsilon_{3\overline{\text{He}}}\left(\langle Q_s \rangle, p_{\text{T}}\right) = \frac{N_{3\overline{\text{He}}}^{TRD}\left(\langle Q_s \rangle > X,\ p_{\text{T}} \in \left[p_{\text{T}}^{thr}, p_{\text{T}}^{thr} + 1\ \text{GeV}/c\right]\right)}{N_{3\overline{\text{He}}}^{ESD}\left(p_{\text{T}} \in \left[p_{\text{T}}^{thr}, p_{\text{T}}^{thr} + 1\ \text{GeV}/c\right]\right)}\ . \tag{15}$$

$\epsilon_{3\overline{\text{He}}}(\langle Q_s \rangle, p_T)$ is an efficiency on track level. This is again a reasonable lower bound approximation for the online efficiency on event level for the same reasons that were discussed previously in section 3.3.

The matching procedure adds another effect to the previosly described tracking efficiency and acceptance (see section 3.3). In Fig. 22a no cut on $\langle Q_s \rangle$ was applied. Hence only the p_T-dependant ratio of $^3\overline{\text{He}}$ candidates that could be matched to a TRD track and all $^3\overline{\text{He}}$ candidates is plotted.
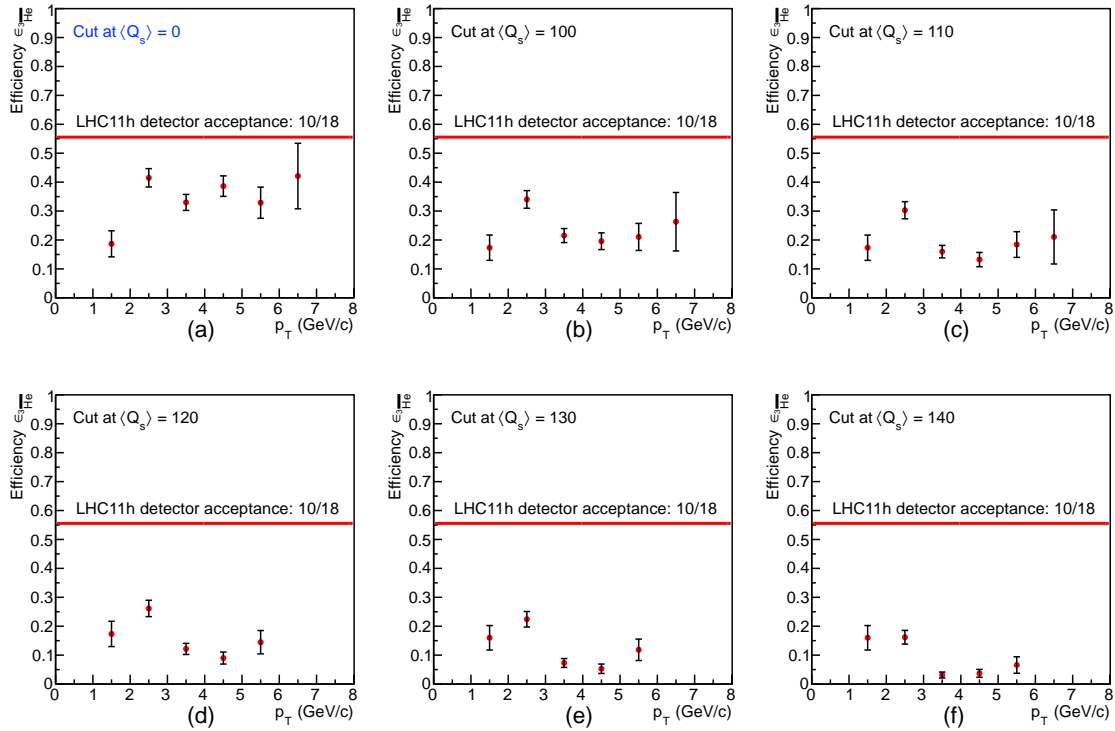

Figure 22: Efficiency $\epsilon_{3\overline{\text{He}}}$ plotted against the transverse momentum for different cuts. In (a) the combined tracking efficiency/acceptance of the TRD and the effect of the track matching is shown since no cut on the scaled charge is applied. The red lines indicate the idealised acceptance since 10 of 18 supermodules were installed during the 2011 PbPb runs. Further losses are mostly due to gaps between the supermodules and edge effects.

Starting at Fig. 15b, with an applied cut at $\langle Q_s \rangle = 100$, the cuts grow in steps of ten, resulting in a maximum cut at $\langle Q_s \rangle = 140$ in Fig. 15f. Similar to the observations in section 3.4 the drop in efficiency is stronger in higher p_T-regions with increasing cuts. Again the p_T-dependence of the energy deposition is the explanation (see section 3.4).

Before the rejection and efficiency can be discussed in combination, it must be taken into account that during the 2011 PbPb runs only 10 of 18 supermodules were installed, whereas during run 176730, which was used for the extraction of the rejection, 13 of 18 supermodules were installed. For the following plots that involve pairs of rejection and efficiency the computed efficiency will therefore be multiplied by a factor of 13/10 to correct the difference in the number of installed supermodules.

To make the results more tangible, the rejection is plotted against the p_T-integrated efficiency for different cuts on $\langle Q_s \rangle$ in Fig. 23. The data point at the lowest rejection results out of a cut at $\langle Q_s \rangle = 170$. With decreasing cuts, going from left to right, the rejection gets worse (approaching 1) and the efficiency increases. The lowest cut was applied at $\langle Q_s \rangle = 70$.
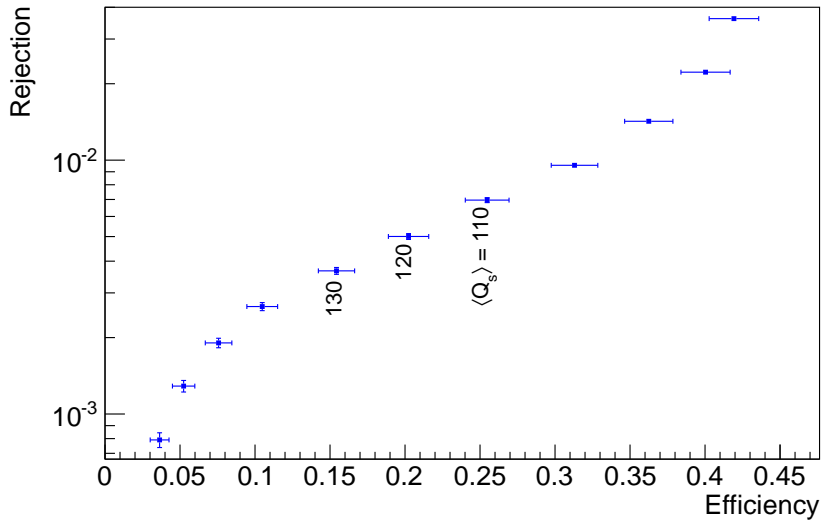

Figure 23: Rejection vs. p_T-integrated $^3\overline{\text{He}}$-efficiency. Each data point represents a certain cut on $\langle Q_s \rangle$.

4.3. Comparison with simulation

In Fig. 24 the p_T-integrated efficiency is plotted against the applied cut on $\langle Q_s \rangle$. The red markers represent the results extracted from the simulated sample, blue markers are based on real data. The results for real data are lower by an average factor of 2.3 in the $\langle Q_s \rangle$-region from 110 to 130. The main source of the observed deviation seems
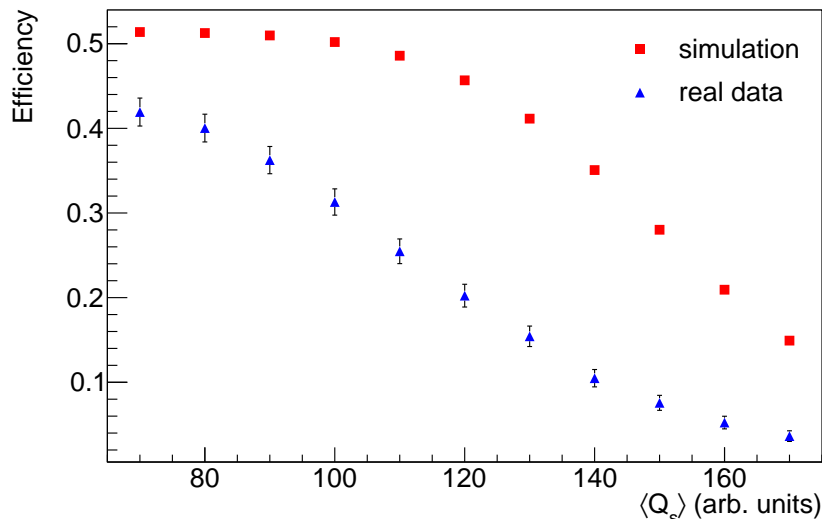

Figure 24: p_T-integrated efficiency vs. the scaled charge for simulated and real data. The results for real data are lower by an average factor of 2.3 in the $\langle Q_s \rangle$-region from 110 to 130.

to be a shift of the energy loss to lower deposited energies in real data compared to the simulation. Fig. 25a, which was already introduced in section 3.1, shows the scaled charge distributions of simulated protons and α-particles, both with a $\beta\gamma$ of 4.25 (resulting in different momenta). Next to that in Fig. 25b a similar plot with different $\beta\gamma$ ranges was extracted from the real data sample. To compare the positions of the peaks and therefore judge the shift in energy deposition, the theoretically expected difference in specific energy loss has to be calculated first.

The momentum of plotted proton tracks ranges from 2 to 3 GeV/c. That translates to a $\beta\gamma$ of about 2 to 3. Since the Bethe curve is nearly flat in that region an average $\beta\gamma$ of 2.5 can be assumed for the plotted proton sample.

In case of $^3\overline{\text{He}}$ every track above 3 GeV/c is used for the plot. Since the p-spectrum is steeply falling it is dominated by tracks close to 3 GeV/c. For a rough approximation one can assume a $\beta\gamma$ of about 1 for the $^3\overline{\text{He}}$ sample.

With these assumptions the theoretically expected shift $\triangle_{theo}$ of the peaks can be calculated and compared to the observed shifts $\triangle_{exp}$ which is done in table 4.

Especially for $^3\overline{\text{He}}$ the obtained numbers are only rough estimates since the theoretical energy deposition is highly dependent on $\beta\gamma$ around a value of 1. Nevertheless we observe a significant shift of the deposited energy towards lower energy deposits. The magnitude of this shift differs between protons and $^3\overline{\text{He}}$ tracks which stands

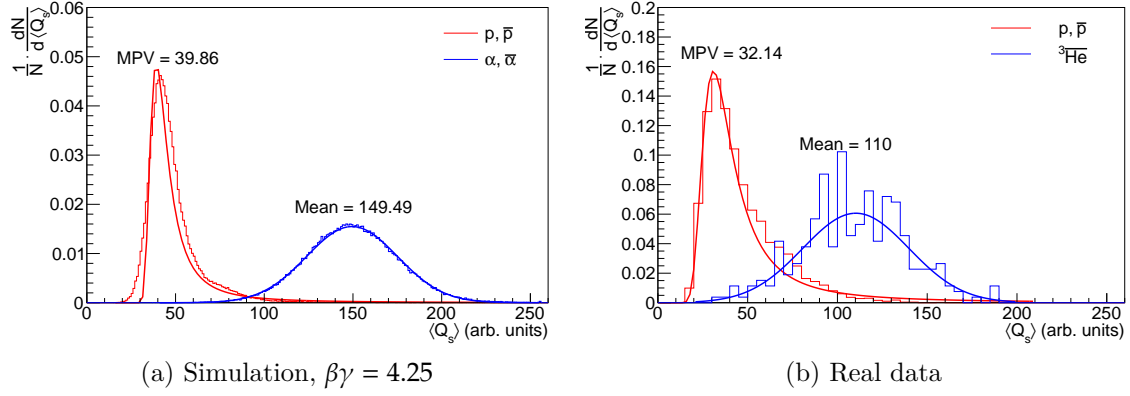(a) Simulation, $\beta\gamma = 4.25$ (b) Real data

Figure 25: a)Scaled charge distributions of protons and α-particles in the TRD, both simulated with $\beta\gamma = 4.25$. Identical to Fig. 13. b) $\langle Q_s \rangle$-distribution of (anti-)protons in the p_T-range of 2 - 3 GeV/c and $^3\overline{\mathrm{He}}$ tracks above 3 GeV/c.

	$\beta\gamma_{theo}$	$\beta\gamma_{exp}$	$\triangle_{theo}$	$\triangle_{exp}$
$p, \overline{p}$	4.25	~ 2.5	-2%	-19%
$^3\overline{\mathrm{He}}$	4.25	~ 1	+20-40%	-26%

Table 4: Shifts of the energy deposit maximum relative to simulated data.

against the hypothesis of a difference in the TRD gain factor as the only difference between simulation and real data.

This large deviation in energy deposition is not fully understood yet and needs further investigation.

5. Conclusion

The goal of this project was to investigate the feasibility of a trigger on light nuclei in p-p collisions with the Transition Radiation Detector in ALICE at the LHC. The mean rate of energy loss of ionizing particles passing through matter, which is described by the Bethe formula, is proportional to the squared charge of the particle. This leads to a high energy deposition in the TRD drift chambers of particles with a charge higher than 1. The main idea of the investigated trigger is to only record events that contain at least one track with a deposited charge/energy higher than a threshold.

The first step in this analysis was to calculate a track-level rejection and efficiency based on a simulated cocktail of electrons, pions, protons, α-particles and their antiparticles with equal abundances and flat p_T-distributions. The analysis resulted in e.g. an α-efficiency of about 44% (acceptance and tracking efficiency of the TRD are included) at an electron rejection of 1/500. The rejection of other particles is stronger. Furthermore, possible improvements of the rejection were investigated. Both approaches, cuts on the transverse momentum and a truncated mean deposited charge, did not improve the rejection significantly.

A strong deviation between the simulated energy deposition of light nuclei and the measured deposition in the TRD was observed. This is still not fully understood and needs further investigation.
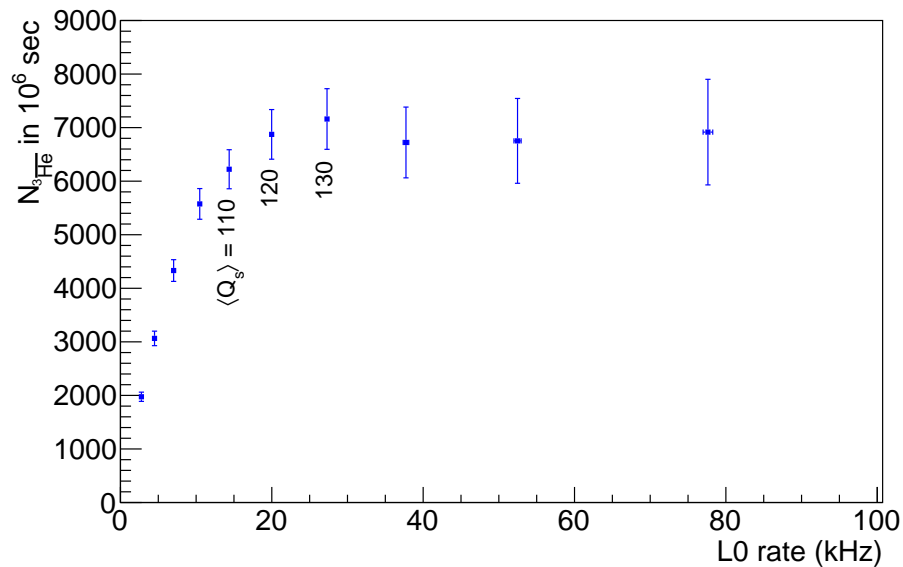

Figure 26: Expected number of recorded $^3\overline{\mathrm{He}}$ tracks if the trigger runs during 10^6 seconds of p-p data taking for different level-0 rates. The number is computed under the assumption of a fixed level-1 rate of 100 Hz and a $^3\overline{\mathrm{He}}$-yield of $1.7 \cdot 10^{-6}$ tracks per event. The combination of level-0 and level-1 rate determines the rejection and therefore the applied cut on $\langle Q_s \rangle$, which this rejection belongs to.

   To achieve significant statistics for the extraction of an efficiency on real data, the PbPb data from 2011 were used. The applied quality and identification cuts resulted in ~890 $^3\overline{\text{He}}$ candidates for efficiency extraction. The rejection could directly be obtained from p-p data. Fig. 26 summarizes the results obtained from real data. If one assumes 10^6 seconds of data taking, which roughly represents 1 month, the expected total number of $^3\overline{\text{He}}$ tracks is plotted versus the L0 rate. The plot was generated under the assumption of a fixed level-1 rate of 100 Hz, so different level-0 rates correspond to certain cuts on the scaled charge which are indicated by the numbers under the data points.
For comparison 10^6 seconds of minimum-bias (no trigger) data taking in p-p at a level-0 rate of 1kHz would lead to approximately 1700 $^3\overline{\text{He}}$ tracks if the same yield is assumed.

   Based on this analysis a trigger on light nuclei seems feasible with the proposed concept. The efficiency was extracted using $^3\overline{\text{He}}$ candidates but is also valid for other (anti-)nuclei with the same or higher charge like the ^{4}He-nucleus. The trigger would also improve the number of detected hypertritons in p-p collisions since they decay to a ^{3}He nucleus and a negative pion. Hypertriton refers to a nucleus composed of a proton, a neutron and a lambda baryon. A lambda baryon is composed of an up, down and strange quark.
The next step is the integration of the trigger decision in the trigger electronics for first test runs. At the beginning of 2013 proton-lead collisions are scheduled at the LHC. Especially due the short data taking period of only 1 month a trigger would be crucial to study the production of light nuclei in proton-lead collisions. Further studies would be necessary to quantify the impact of different multiplicities and other effects on the trigger performance.

A. Config.C of simulation

```
1          Double_t ptmin = 0.;
2          Double_t ptmax = 10.;
3          Double_t ymin  = -1.5;
4          Double_t ymax  = 1.5;
5
6          Int_t nPart = 10;
7
8          AliGenCocktail* gener = new AliGenCocktail();
9          gener->SetProjectile("p", 1, 1);
10         gener->SetTarget("p", 1, 1);
11         gener->SetEnergyCMS(energy);
12         gener->UsePerEventRates();
13         gener->SetPtRange(ptmin, ptmax);
14         gener->SetYRange(ymin, ymax);
15         gener->SetMomentumRange(0., 999999.);
16
17         AliGenBox* alpha = new AliGenBox(nPart);
18         alpha->SetPart(1000020040);
19         alpha->SetPtRange(ptmin, 2.*ptmax);
20         gener->AddGenerator(alpha, "alpha", 1);
21
22         AliGenBox* antialpha = new AliGenBox(nPart);
23         antialpha->SetPart(-1000020040);
24         antialpha->SetPtRange(ptmin, 2.*ptmax);
25         gener->AddGenerator(antialpha, "antialpha", 1);
26
27         AliGenBox* proton = new AliGenBox(nPart);
28         proton->SetPart(2212);
29         gener->AddGenerator(proton, "proton", 1);
30
31         AliGenBox* antiproton = new AliGenBox(nPart);
32         antiproton->SetPart(-2212);
33         gener->AddGenerator(antiproton, "antiproton", 1);
34
35         AliGenBox* electron = new AliGenBox(nPart);
36         electron->SetPart(11);
37         gener->AddGenerator(electron, "electron", 1);
38
39         AliGenBox* positron = new AliGenBox(nPart);
40         positron->SetPart(-11);
41         gener->AddGenerator(positron, "positron", 1);
42
43         AliGenBox* piplus = new AliGenBox(nPart);
44         piplus->SetPart(211);
45         gener->AddGenerator(piplus, "piplus", 1);
46
47         AliGenBox* piminus = new AliGenBox(nPart);
48         piminus->SetPart(-211);
49         gener->AddGenerator(piminus, "piminus", 1);
```

Listing 1: Part of the Config.C where the simulated cocktail is composed.

B. Track cuts on real data

```
1  AliESDtrackCuts::GetStandardITSTPCTrackCuts2011(Bool_t selPrimaries,
2                                                   Int_t clusterCut)
3  {
4     AliInfoClass("Creating track cuts for ITS+TPC (2011 definition).");
5
6     AliESDtrackCuts* esdTrackCuts = new AliESDtrackCuts;
7
8     // TPC
9     if(clusterCut == 0)   esdTrackCuts->SetMinNClustersTPC(50);
10    else if (clusterCut == 1) {
11       esdTrackCuts->SetMinNCrossedRowsTPC(70);
12       esdTrackCuts->SetMinRatioCrossedRowsOverFindableClustersTPC(0.8);
13    }
14    else {
15       esdTrackCuts->SetMinNClustersTPC(50);
16    }
17    esdTrackCuts->SetMaxChi2PerClusterTPC(4);
18    esdTrackCuts->SetAcceptKinkDaughters(kFALSE);
19    esdTrackCuts->SetRequireTPCRefit(kTRUE);
20    // ITS
21    esdTrackCuts->SetRequireITSRefit(kTRUE);
22    esdTrackCuts->SetClusterRequirementITS(AliESDtrackCuts::kSPD,
23                                            AliESDtrackCuts::kAny);
24    if(selPrimaries) {
25       // 7*(0.0015+0.0050/pt^1.1)
26       esdTrackCuts->SetMaxDCAToVertexXYPtDep("0.0105+0.0350/pt^1.1");
27       esdTrackCuts->SetMaxChi2TPCConstrainedGlobal(36);
28    }
29    esdTrackCuts->SetMaxDCAToVertexZ(2);
30    esdTrackCuts->SetDCAToVertex2D(kFALSE);
31    esdTrackCuts->SetRequireSigmaToVertex(kFALSE);
32
33    esdTrackCuts->SetMaxChi2PerClusterITS(36);
34
35    return esdTrackCuts;
36 }
```

Listing 2: Used track cuts.

C. ALEPH parameters

$$\lambda_1 = 1.4906$$
$$\lambda_2 = 27.9758$$
$$\lambda_3 = 4.00313 \cdot 10^{-15}$$
$$\lambda_4 = 2.50804$$
$$\lambda_5 = 8.31768$$

Table 5: ALEPH parameters for $^{3/4}$He, PbPb 2011 (pass2)

Acknowledgments

References

[1]   Peter Braun-Munzinger and Johanna Stachel. "The quest for the quark-gluon plasma". In: *Nature* 448 (2007), pp. 302–309.

[2]   J. Cleymans et al. "Antimatter production in proton-proton and heavy-ion collisions at ultrarelativistic energies". In: *Phys.Rev.* C84 (2011), p. 054916. arXiv:1105.3719 [hep-ph].

[3]   H. Agakishiev et al. "Observation of the antimatter helium-4 nucleus". In: *Nature* 473 (2011), p. 353. arXiv:1103.3312 [nucl-ex].

[4]   Alexander Kalweit. Private communication.

[5]   Natasha Sharma. Private Communication.

[6]   Helmut Öschler. "Production of Strange Particles from the Lowest to the Highest Energies". Strangeness in Quark Matter, September 2011, Cracow.

[7]   Lyndon Evans (ed.) and Philip Bryant (ed.). "LHC Machine". In: *JINST* 3 (2008), S08001.

[8]   G. Aad et al. "The ATLAS Experiment at the CERN Large Hadron Collider". In: *JINST* 3 (2008), S08003.

[9]   S. Chatrchyan et al. "The CMS experiment at the CERN LHC". In: *JINST* 3 (2008), S08004.

[10] Jr. Alves A. Augusto et al. "The LHCb Detector at the LHC". In: *JINST* 3 (2008), S08005.

[11] K. Aamodt et al. "The ALICE experiment at the CERN LHC". In: *JINST* 3 (2008), S08002.

[12] Jochen Klein. "Commissioning of and Preparations for Physics with the Transition Radiation Detector in A Large Ion Collider Experiment at CERN." Diploma thesis. University of Heidelberg, 2008.

[13] Alexander Kalweit. "Production of light flavor hadrons and anti-nuclei at the LHC". PhD thesis. TU Darmstadt, July 2012.

[14] Thomas Bird. *An Overwiew of the ALICE Experiment.* 2010.

[15] ALICE Collaboration. ALICE TRD Technical Design Report. Technical Report CERN/LHCC 2001-021, CERN, 2001.

[16] Yvonne Pachmayer. "Physics with the ALICE Transition Radiation Detector". In: *Nuclear Instruments and Methods in Physics Research Section A: Accelerators, Spectrometers, Detectors and Associated Equipment* (2012), ISSN: 0168-9002. URL: http://www.sciencedirect.com/science/article/pii/S0168900212005037.

[17] Jochen Klein. "Triggering with the ALICE TRD". In: *Nuclear Instruments and Methods in Physics Research Section A: Accelerators, Spectrometers, Detectors and Associated Equipment* (2012), ISSN: 0168-9002. URL: `http://www.sciencedirect.com/science/article/pii/S0168900212004986`.

[18] Jan de Cuveland. "A Track Reconstructing Low-latency Trigger Processor for High-energy Physics". PhD thesis. University of Heidelberg, 2009.

[19] *AliRoot*. URL: `http://alisoft.cern.ch/`.

[20] *ROOT*. URL: `http://root.cern.ch/`.

[21] *Pythia 6*. URL: `http://pythia6.hepforge.org/`.

[22] *Geant 3*. URL: `http://wwwasd.web.cern.ch/wwwasd/geant/`.

[23] *AliAnalysis Framework*. URL: `http://aliweb.cern.ch/Offline/Activities/Analysis/index.html`.

[24] J. Beringer et al. (Particle Data Group). *Phys. Rev. D86, 010001*. 2012.

[25] Nicole Martin. "Investigation of light (anti-)nuclei and (anti-)hypernuclei with ALICE at the LHC (CERN)". MA thesis. TU Darmstadt, 2011.

[26] Alexander Kalweit and Marian Ivanov. "TPC Gain Calibration and Particle Identification". Alice offline week, July 2008.

[27] Nicole Martin. Private communication.

Erklärung

Ich versichere, dass ich diese Arbeit selbstständig verfasst und keine anderen als die angegebenen Quellen und Hilfsmittel benutzt habe.

Heidelberg, den